Electronic Supplementary Information (ESI)

Conjugation-Interrupted Polyimides with Amplified Local Electric Fields for SF_6/N_2 Separation

Jiangli Zhu,[a] Qilin Wang,[a] and Jun Yan*[a,b]

[a]*School of Materials Science and Engineering, North Minzu University, Yinchuan 750021, China*

[b]*Institute of Functional and Structural Characteristic Materials, Helanshan Laboratory, Yinchuan 750021, China*

Corresponding Authors:

*E-mail: yanjun2018@nun.edu.cn (Jun. Yan)

Experimental Section

Materials.

1,3,5-tris(4-aminophenyl)benzene (TAPB) (97%), 4,4',4",4"'-(pyrene-1,3,6,8-tetrayl) tetraaniline (TAPPy) (98%), and 5"-(4'-amino-[1,1'-biphenyl]-4-yl)-[1,1':4',1":3",1"':4"',1""-quinquephenyl]-4,4""-diamine (TAPQ) (98%) were purchased from Zhengzhou Alfa Chemical Co., Ltd. Bicyclo[2.2.2]oct-7-ene-2,3,5,6-tetracarboxylic dianhydride (BCO-TDA) (98%), *m*-Cresol (99%), isoquinoline (97%), dimethyl sulfoxide (DMSO, 99%), *N,N*-dimethylformamide (DMF, 99%), and anhydrous tetrahydrofuran (THF) were supplied by J&K Chemical Co., Ltd. and used as received.

Experimental Methods.

Synthesis of MCPIs.

All three semicycloaliphatic polyimide networks were prepared by an analogous procedure;[1] MCPI-1 is described here as a representative example. Under an argon atmosphere, a mixture of 1,3,5-tris(4-aminophenyl)benzene (0.491 g, 1.4 mmol), bicyclo[2.2.2]oct-7-ene-2,3,5,6-tetracarboxylic dianhydride (0.521 g, 2.1 mmol), and *m*-cresol (20 mL) was stirred at 60 ℃ until a homogeneous solution was obtained. After the addition of isoquinoline (1.0 mL), the mixture was heated stepwise from 120 ℃ to 220 ℃ (4 h at each stage, with 20 ℃ increments between stages). The precipitate was collected by filtration, washed successively with DMSO, DMF, and THF, and further extracted via Soxhlet extraction (THF, 3 days). The product was dried under vacuum at 80 ℃ to give MCPI-1 as a white powder (yield: 88%).

Material Characterization

The morphologies of the as-prepared polymers were examined by field-emission scanning electron microscopy (FE-SEM) using a ZEISS SUPRA™ 55 microscope. Transmission electron microscopy (TEM) images were acquired on a FEI Talos F200X microscope (Thermo Fisher Scientific). Powder X-ray diffraction (PXRD) patterns were recorded on a Rigaku D/Max 2400 diffractometer with Cu K_α radiation (λ = 1.5406 Å) at a scan rate of 2°·min^{-1}. Thermogravimetric analysis (TGA) was performed on a TA Instruments Q50 analyzer. Samples were heated from room temperature to 800 °C at 10 °C·min^{-1} under a continuous N_2 flow. The chemical structures of the as-prepared polymers were characterized by Fourier-transform infrared (FTIR) spectroscopy on a Nicolet™ 20XB spectrometer (Thermo Fisher Scientific). Solid-state ^{13}C cross-polarization/total sideband suppression (CP/TOSS) NMR spectra were recorded on a Bruker AVANCE III HD 600 MHz spectrometer. N_2 physisorption isotherms at 77 K were measured on a Quantachrome Instruments Autosorb-iQ3 analyzer. Single-component adsorption isotherms for N_2 and SF_6 were measured at 273 and 298 K using a BSD-PMC volumetric adsorption analyzer (BeiShiDe Instrument). IAST selectivities for SF_6/N_2 mixtures (10/90, v/v) were calculated based on fitting the pure-component isotherms to a single-site Langmuir-Freundlich model. Dynamic breakthrough experiments were performed at 298 K in a fixed-bed quartz column (0.6 cm ID × 7.5 cm) packed with approximately 0.20 g of the adsorbent. Prior to each experiment, the sample was activated in situ by heating at 373 K under a He flow (20 mL·min^{-1}) for 3 h. A gas mixture of SF_6/N_2 (10/90, v/v) was then introduced at a total flow rate of 5 mL·min^{-1}. The composition of the effluent gas was monitored by a Pfeiffer Vacuum ThermoStar mass spectrometer, tracking the ion signals at m/z = 89 for SF_6 and 28 for N_2.

Fitting of experimental data on pure component isotherms

The single-component adsorption isotherms of SF_6 and N_2 on MCPIs were fitted at 273 K and 298 K to the single-site Langmuir-Freundlich model (equation S1).

$$\mathrm{N} = \mathrm{A}\frac{\mathrm{B} \times P^{C}}{1 + B \times P^{C}} \qquad S1$$

where N is the adsorption capacity (mmol·g^{-1}), P is the pressure (kPa), A is the saturated adsorption capacity (mmol·g^{-1}), B is the affinity coefficient (kPa^{-C}), and C is the Langmuir-Freundlich exponent (dimensionless).

IAST selectivity calculation

To benchmark the SF_6/N_2 separation performance of MCPIs, mixture adsorption equilibria were evaluated by IAST calculations. For a binary mixture of components A and B, the governing equations based on equal spreading pressures were solved numerically to determine the mole fractions and equilibrium loadings of each component in the adsorbed phase.[1] The adsorption selectivity was determinde was then determined according to equation S2.

$$S_{a\ b\ \bar{s}} = \frac{q_A / q_B}{y_A / y_b} \qquad S2$$

The separation potential (Δq), a composite metric that integrates both adsorption capacity and selectivity, was adopted to assess adsorbent performance following the framework proposed by Krishna.[2, 3] The productivity of pure SF_6 recoverable during the desorption step of a fixed-bed cycle is given by equation S3.

$$\Delta\ q = q\ 1 \times {}^{y\ 2}/_{y\ 1} - q\ 2 \qquad S3$$

where y1 and y2 are the mole fractions of components 1 and 2 in the gas phase, and q1 and q2 are the corresponding equilibrium loadings in the adsorbed phase predicted by IAST at the respective partial pressures. Owing to competitive co-adsorption, q1 and q2 deviate from the values derived from the pure-component isotherms.

Estimation of the Isosteric heats of SF_6 and N_2 gas adsorption

The isosteric enthalpies of adsorption for SF_6 and N_2 on MCPIs were determined by the virial-type thermal equation using data collected at 273 and 298 K.[4] The experimental data were fitted to equation S4 in each case.

$$\ln(P) = \ln(N) + 1/T \sum_{i=0}^{m} a_i N^i + \sum_{i=0}^{m} b_i N^i \qquad S4$$

Here, P is the pressure expressed in mmHg, N is the quantity adsorbed in mg/g, T is the temperature in K, a_i and b_i are virial coefficients, m and n represent the number of coefficients required to adequately describe the isotherms (m and n denote the number of virial coefficients retained for an adequate fit. Both were incrementally increased until additional a and b terms made no statistically significant improvement to the residual sum of squares). The values of the virial coefficients through am were then used to calculate the isosteric heat of adsorption using the following expression (equation S5).

The virial coefficients a_0 through a_m were then substituted into equation S5 to obtain the isosteric heat of adsorption.

$$Q_{st} = -R \sum_{i=0}^{m} a_i N^i \qquad S5$$

where Q_{st} is the coverage-dependent isosteric heat of adsorption and R is the universal gas constant (8.314 $J \cdot K^{-1} \cdot mol^{-1}$).

Breakthrough

The adsorption amount of adsorbent n is calculated according to the equation S6 as:

$$Q_{nad} = Q_{nin} - Q_{nout} = q_{in} \times C_{n0} \times \Delta T - \int_{0}^{t} [q/(1 - \sum_{1}^{N} C_{nt}))] * C_{nt} dt \qquad S6$$

Q_{nad} is the adsorption amount of adsorbent n; Q_{nin} is the total flow rate of adsorbent n flowing in of the penetrating column at ΔT; Q_{nout} is the total flow rate of adsorbent n flowing out of the penetrating column at ΔT; q_{in} is the total flow rate of gas through the column inlet; C_{n0} is the total flow rate of gas through the outlet of the column; ΔT is the total adsorption time (min); q is the flow rate of carrier gas; C_{nt} is the percentage concentration of adsorbent N at the entrance of the penetrating column;

Computational details

All calculations were carried out within the Materials Studio 2020 suite. Geometries of the monomer building blocks and representative polymer fragments were first pre-optimized with the Forcite module to generate physically reasonable starting conformations. The Universal Force Field (UFF) was adopted with the quasi-Newton optimizer and a convergence limit of 500 steps; all remaining parameters were set to their default values. This force-field pre-optimization served to eliminate unreasonable bond lengths, valence angles, and steric clashes, thereby furnishing reliable initial structures for the subsequent density functional theory (DFT) refinement. Refined geometry optimizations were then performed at the DFT level using the DMol^3 module. The exchange‑correlation functional was treated within the generalized gradient approximation (GGA) using the Perdew–Burke–Ernzerhof (PBE) parameterization, supplemented by the DFT-D empirical dispersion correction to capture van der Waals interactions. The adsorption energy (ΔE_{ads}) calculation was performed using the molecular mechanics (MM) calculations. Initially, the

structures of the adsorbates (SF_6 and N_2) and MCPIs were optimized using the geometry optimization task with the Universal Forcefield. Subsequently, the binding structure of the adsorbates with MCPIs was constructed and optimized to calculate ΔE_{ads}, again utilizing the geometry optimization task with the Universal Forcefield. Finally, the value of ΔE_{ads} was computed using the energy task with the Universal Forcefield. The adsorption energy was estimated as follows:

$$\Delta E_{ads} = E_{complex} - (E_{host} + E_{guest}) \quad \text{S7}$$

Where ΔE_{ads} represent the adsporption energy, $E_{complex}$, E_{guest} and E_{host} are the total energies of the polymer with the gas molecule, the energy of the gas molecule, and the energy of the material, respectively.

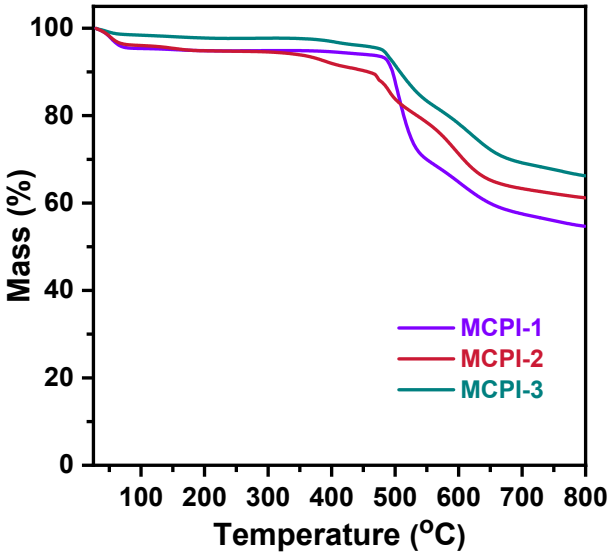

Figure S1. TGA curves of MCPIs under nitrogen atmospheres.

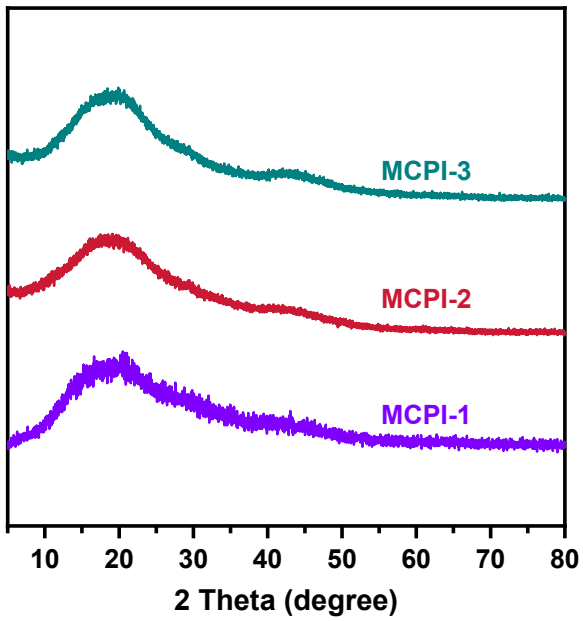

Figure S2. Wide-angle X-ray diffraction (WAXD) patterns of MCPIs.

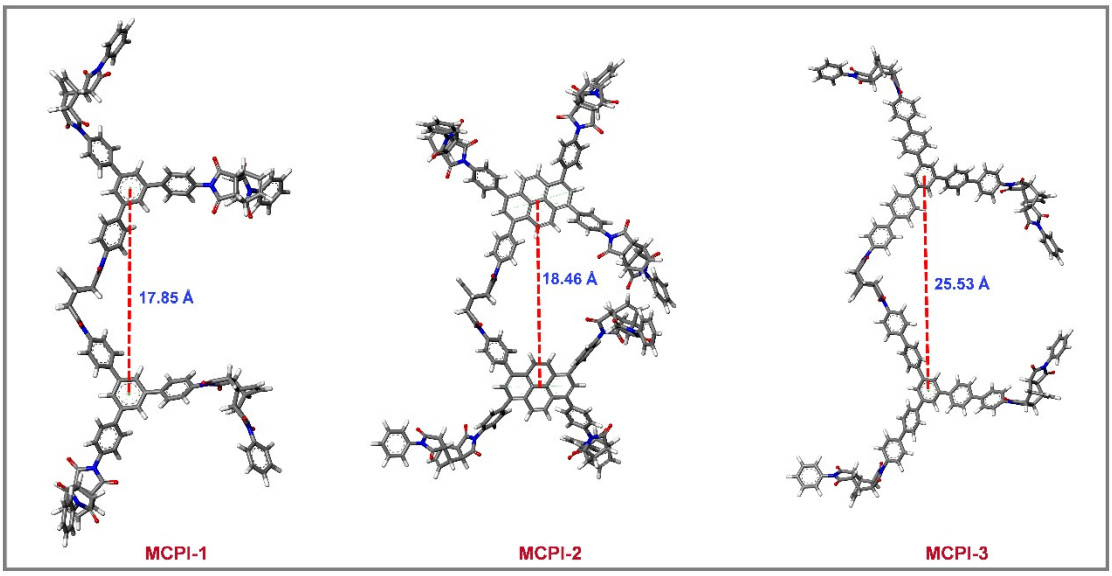

Figure S3. Atomistic simulation snapshots of representative fragments of MCPI-1, MCPI-2, and MCPI-3.

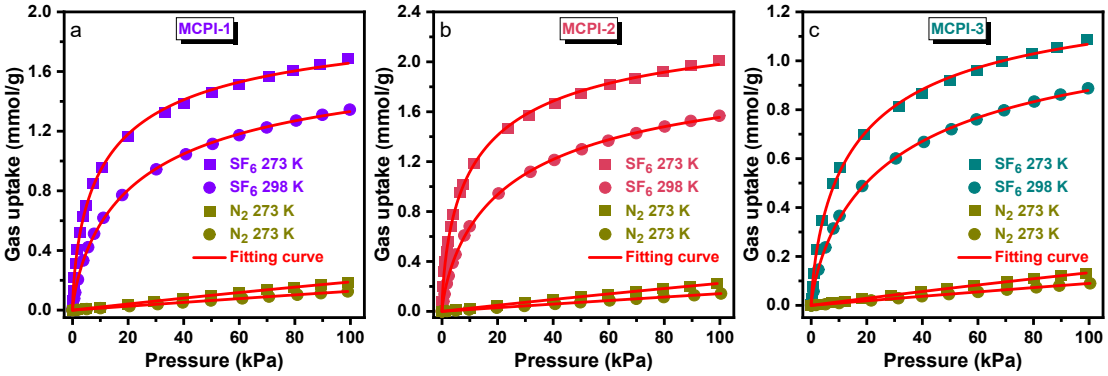

Figure S4. Adsorption isotherms and single-site Langmuir-Freundlich fitting curves for SF_6 and N_2 in MCPIs at 273 K and 298 K.

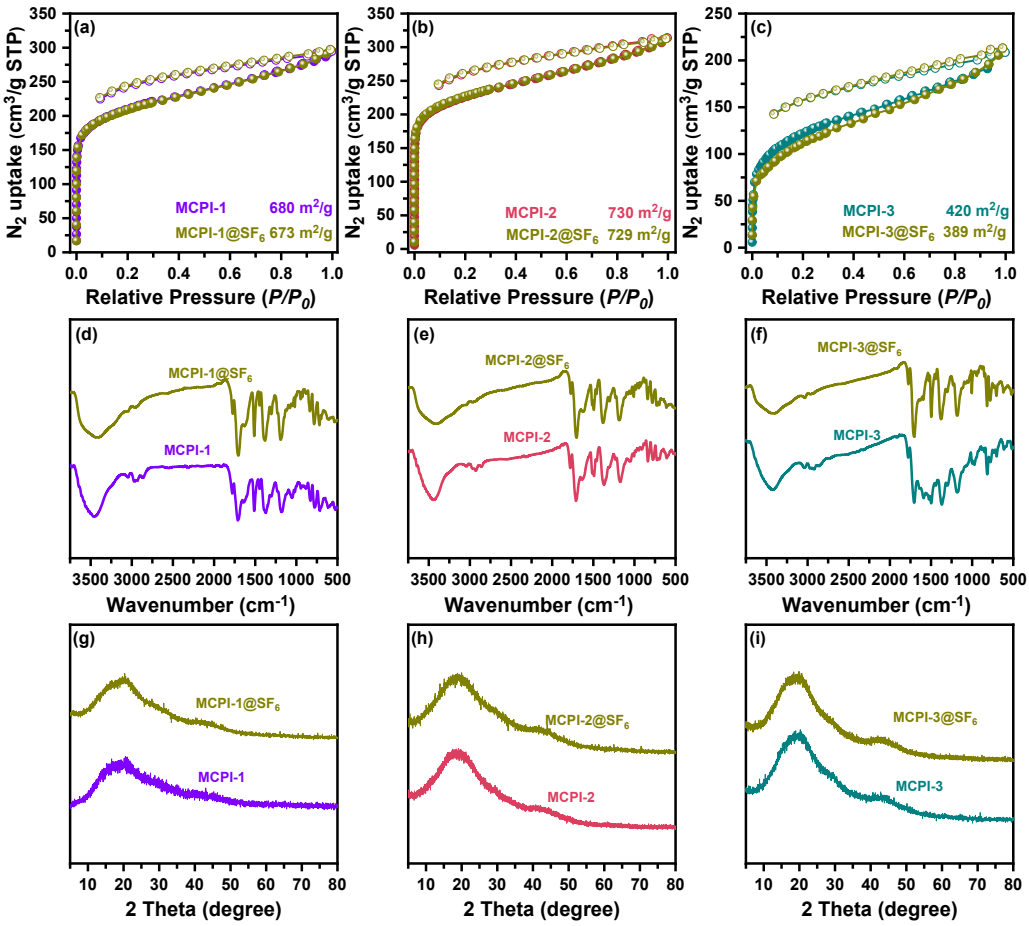

Figure S5.(a-c) N_2 adsorption-desorption isotherms at 77 K; (d-f) FTIR spectra of MCPIs before and after SF_6 adsorption; (g-i) WAXD patterns of MCPIs before and after SF_6 adsorption.

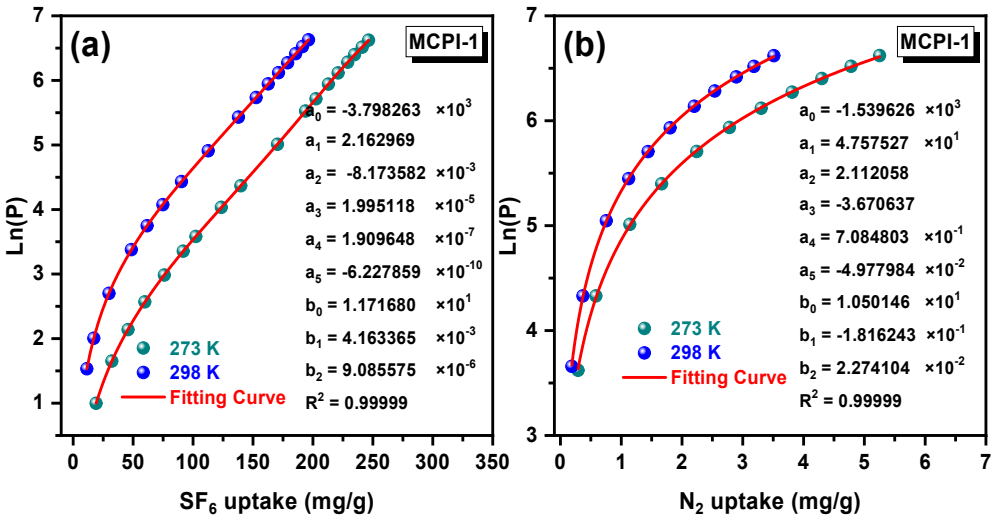

Figure S6. Virial equation fitting of SF_6 and N_2 adsorption isotherm of MCPI-1.

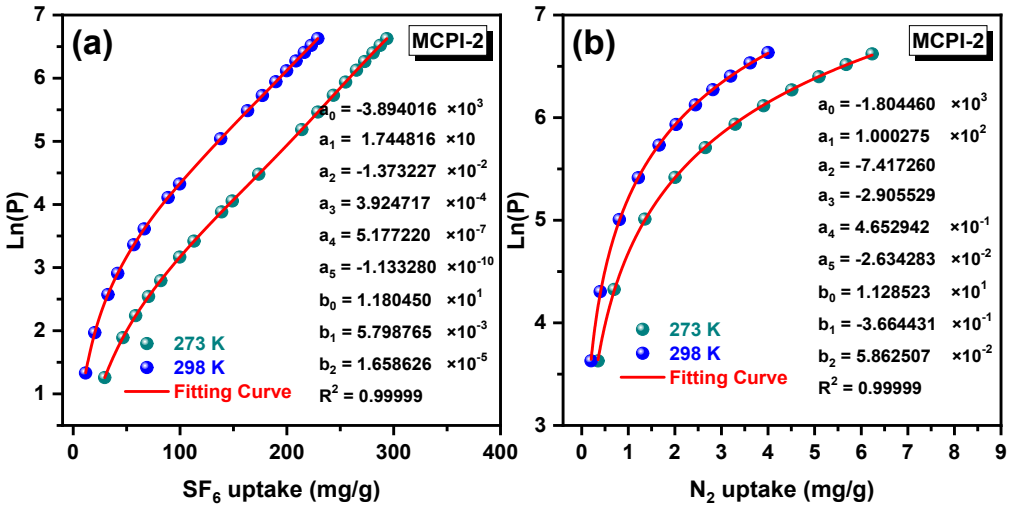

Figure S7. Virial equation fitting of SF_6 and N_2 adsorption isotherm of MCPI-2.

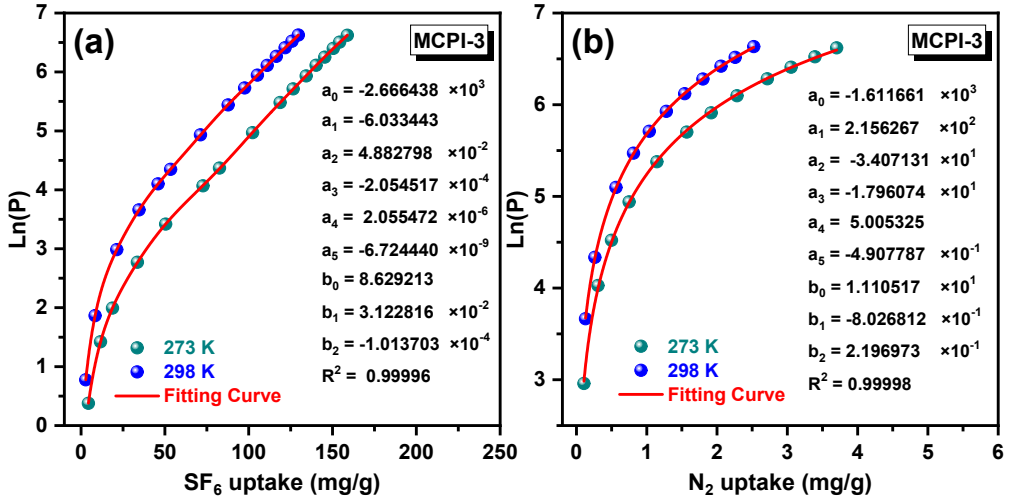

Figure S8. Virial equation fitting of SF_6 and N_2 adsorption isotherm of MCPI-3.

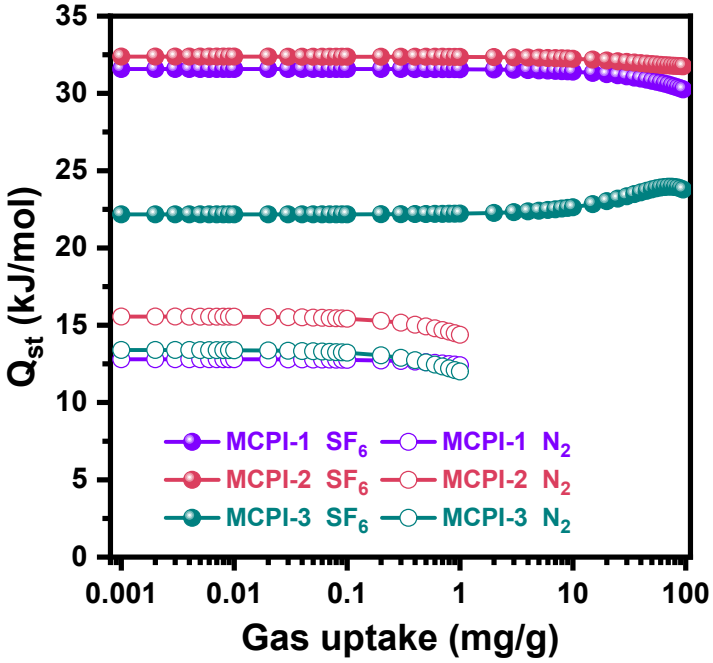

Figure S9. Isosteric heat of adsorption for SF_6 and N_2 of MCPIs.

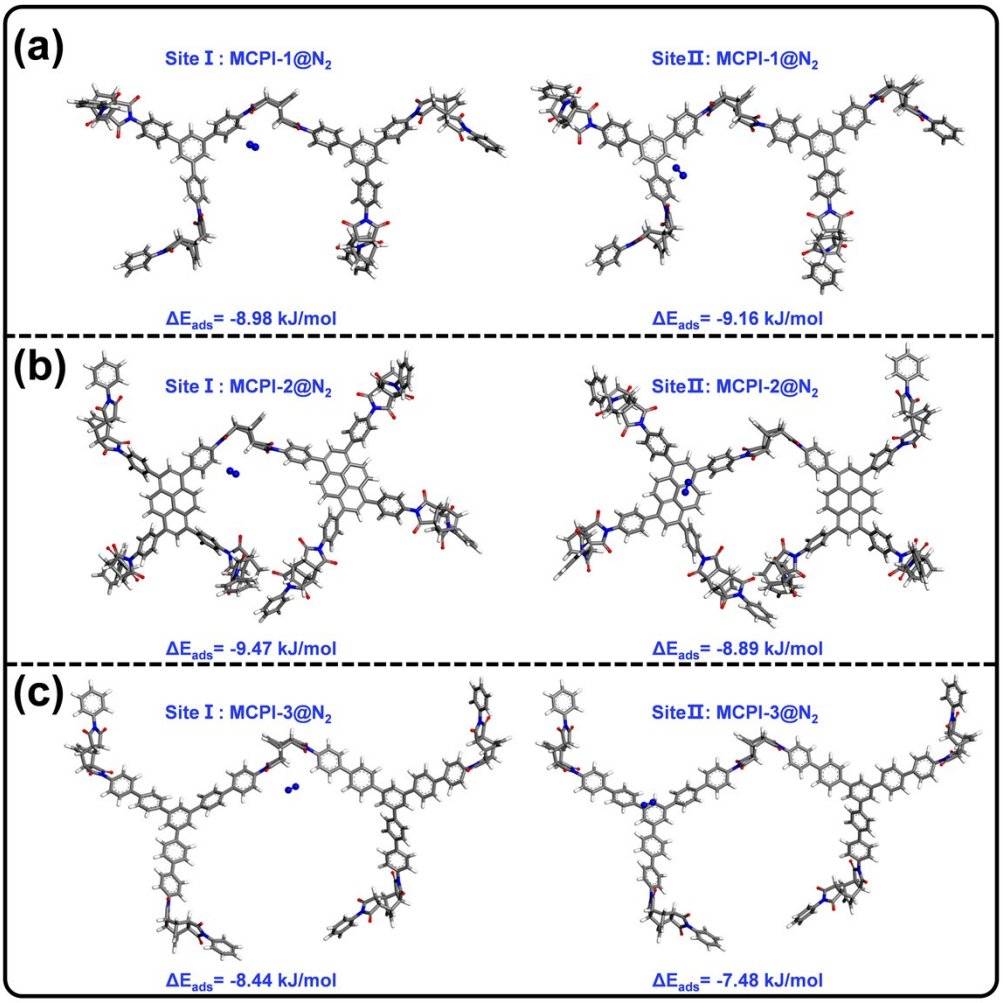

Figure S10. DFT-calculated adsorption configurations and binding energies of N_2 and at sites I and site II in MCPI-1 (a), MCPI-2 (b), and MCPI-3 (c).

Table S1. The chemical composition of MCPIs based on elemental analysis

Samples	Experimental (wt%)				Theoretical (wt%)			
	C	N	O	H	C	N	O	H
MCPI-1	68.8	5.5	21.0	4.7	75.33	6.27	14.33	4.06
MCPI-2	70.4	4.8	20.1	4.7	74.84	5.46	15.58	4.12
MCPI-3	75.0	4.1	16.3	4.6	79.72	4.65	10.62	5.02

Table S2. The porosity parameters of MCPIs

Samples	S_{BET} （$m^2 \cdot g^{-1}$） [a]	S_{micro} （$m^2 \cdot g^{-1}$） [b]	V_{micro} （$mL \cdot g^{-1}$） [b]	V_{total} （$mL \cdot g^{-1}$） [c]
MCPI-1	680	502	0.25	0.46
MCPI-2	730	558	0.28	0.49
MCPI-3	420	324	0.19	0.32

[a]Calculated using BET theory. [b]Calculated by the t-plot method. [c]Determined from N_2 adsorption isotherms at P/P_0 = 0.99.

Table S3. Single-site Langmuir-Freundlich simulated parameters for MCPIs

Sample	T/K	Gas	A(mmol/g)	B(kPa^{-C})	C	R^2
MCPI-1	273	SF_6	2.0645	1.6189×10^{-1}	0.6921	0.9993
		N_2	1.9237	1.0976×10^{-3}	0.9984	0.9999
	298	SF_6	1.7645	7.8831×10^{-2}	0.7916	0.9998
		N_2	0.8941	1.2599×10^{-3}	1.0561	0.9999
MCPI-2	273	SF_6	2.4733	1.6943×10^{-1}	0.6873	0.9994
		N_2	2.6775	9.5779×10^{-4}	0.9901	0.9999
	298	SF_6	2.1404	7.8534×10^{-2}	0.7648	0.9998
		N_2	1.4047	9.4812×10^{-4}	1.0362	0.9999
MCPI-3	273	SF_6	1.3593	1.1751×10^{-1}	0.7476	0.9992
		N_2	1.3630	1.0881×10^{-3}	0.9945	0.9999
	298	SF_6	1.2505	6.4503×10^{-2}	0.7827	0.9997
		N_2	0.9234	9.3065×10^{-4}	1.0313	0.9999

Table S4. Comparison of adsorption characteristics of porous materials for SF_6/N_2 separation at 298 K and 100 kPa.

Materials	S_{BET} ($m^2 \cdot g^{-1}$)	SF_6 uptake ($mmol \cdot g^{-1}$)		IAST selectivity (10:90) SF_6/N_2	SF_6 Q_{st} (kJ/mol)	Ref
		273 K	298 K			
MCPI-1	680	1.69	1.34	100	30.3	
MCPI-2	730	2.01	1.57	96	31.5	This work
MCPI-3	420	1.09	0.89	69	23.8	
NMUCOF-1	991	1.76	1.11	37	26.6	5
NMUCOF-2	1630	2.57	1.45	36	22.8	6
NMUCOF-3	851	1.99	1.25	53	26.6	6
NMUCOF-4	631	1.96	1.63	113	29.1	6
NMUCOF-5	751	2.42	1.90	126	30.2	6
ACOF-1	831	2.57	2.15	54	-	7
FCOF-1	1885	2.21	1.08	14	-	7
KFCOF-1	744	1.58	0.99	32	-	7
RCOF-1-5	428	1.41	1.11	52	30.0	7
RCOF-2	763	2.41	1.86	45	25.1	7
RCOF-3	242	0.91	0.58	25	21.4	7
COF-300	1106	4.03	3.09	51	-	7
RCOF-1	1139	4.13	3.46	83	27.0	7
RCOF-1-2	984	3.47	2.97	78	33.2	7
RCOF-1-3	945	3.30	2.49	88	27.7	7
RCOF-1-4	864	3.11	2.42	88	29.2	7
BrCOF-2	1602	-	~1.3	~17	20.6	8
BrCOF-2-CF_3	1514	-	1.45	39	24.8	8
3D-TMTAPB-COF	940	-	~2.72	335	-	9
CNOP-7	1270	2.60	1.90	73	30	10
ANOP-8	694	0.92	0.80	51	26	11
TNOP-1	822	2.08	1.59	84.7	30	12
TNOP-2	605	1.12	0.92	77	26.6	13
TNOP-3	803	1.67	1.28	98	33.1	13
TNOP-4	891	2.13	1.62	105	33.5	13
TNOP-5	772	1.74	1.34	108	35.5	13
PKAN-1	977	2.97	2.40	113	29.3	14
POPTrB-4F	775.5	2.88	-	62.88[a]	30.25	15
POPTrB-8F	628.9	2.21	-	51.55[a]	27.15	15
PAF-4F	1071.9	2.46	-	38.58[a]	30.4	16
PAF-8F	818.3	1.90	-	50.89[a]	30.0	16
PAF-XJTU-1	2025	-	5.35	47.18	24.04	17
PAF-XJTU-2	1924	-	4.83	46.64	33.64	17
PAF-XJTU-3	1499	-	4.60	36.76	31.03	17
PAF-XJTU-4	1419	-	3.34	29.39	25.08	17
$Zn(BDC)(DABCO)_{0.}$	1978.1	-	3.48	31.8	-	18

[5] Zn(DMBDC)$(DABCO)_{0.5}$	1336.1	-	4.77	118.9	-	18
Zn(TMBDC)$(DABCO)_{0.5}$	975.9	-	4.61	239	-	18
ZIF-7	396	-	0.46	22.1[b]		19
ZIF-8	1540	-	0.15	1.7[b]	-	19
$Cu(peba)_2$	814.3	-	2.36	18.2	14.4	20
Ni(pba)2	807	-	3.50	200.6	24	20
Ni(ina)2	470	-	2.84	375.1	33.40	20
SNNU-202	1319	-	4.94	9	20.0	21
SNNU-203	1522	-	5.6	27	20.8	21
SNNU-204	2170	-	6.06	49	21	21
PAF-2,4diF-DBrM	1004.53		~1.3	52.00	19.67	22
PAF-2F-DBrM	1364.03		~2.6	99.04	28.53	22
PAF-4,4diF- DBrM	1392.37		~2.2	85.73	28.99	22
PAF-4F-DBrM	1408.37		~2.9	195.70	28.98	22
PAF-3,3diF- DBrM	1299.66		~3.0	113.02	29.87	22
CPOF-12	1140		2.20	149.4	26.8	23

[a]SF_6/N_2=1:99; [b]IAST selectivity in 293 K

Table S5. Breakthrough time, dynamic adsorption uptake, and mass-transfer-zone velocity of SF_6 and N_2 derived from fixed-bed breakthrough experiments at 298 K.

Samples	Gas	Breakthrough time (s/g)	Breakthrough adsorption Uptake (cm^3/g)	Static adsorption Uptake (cm^3/g)	Flow velocity of MTZ (cm/s)
MCPI-1	SF_6	1104.2	12.66	13.06	0.0047
	N_2	19.8	2.36	2.54	0.1292
MCPI-2	SF_6	1079.3	15.57	15.26	0.0048
	N_2	12.0	2.51	2.89	0.1409
MCPI-3	SF_6	156.0	5.51	8.12	0.0122
	N_2	12.1	2.50	1.81	0.1360

References

1. J. Yan, B. Zhang and Z. Wang, Monodispersed ultramicroporous semi-cycloaliphatic polyimides for the highly efficient adsorption of CO_2, H_2 and organic vapors, *Polym. Chem.*, 2016, **7**, 7295-7303.
2. R. Krishna, Metrics for Evaluation and Screening of Metal–Organic Frameworks for Applications in Mixture Separations, *ACS Omega*, 2020, **5**, 16987-17004.
3. L. Wang, W. Sun, Y. Zhang, N. Xu, R. Krishna, J. Hu, Y. Jiang, Y. He and H. Xing, Interpenetration Symmetry Control Within Ultramicroporous Robust Boron Cluster Hybrid MOFs for Benchmark Purification of Acetylene from Carbon Dioxide, *Angew. Chem. Int. Ed.*, 2021, **60**, 22865-22870.
4. L. Czepirski and J. JagieŁŁo, Virial-type thermal equation of gas-solid adsorption, *Chem. Eng. Sci.*, 1989, **44**, 797-801.
5. J. Zhu, Q. Wang, Z. Wang and J. Yan, Fluorinated Imide-Linked Covalent Organic Framework for Selective SF_6 Capture and Separation, *ACS Appl. Polym. Mater.*, 2025, **7**, 9488-9495.
6. J. Yan, J. Zhu, Q. Wang and s. Guo, Tunable Methylation in Imide-Linked Covalent Organic Frameworks Enables Highly Selective SF_6 Capture, *J. Am. Chem. Soc.* , 2026, DOI: 10.1021/jacs.6c02143.
7. Q. Liao, H. Xu, C. Ke, Y. Zhang, Q. Han, Y. Zhang, Y. Xu, D. Wang and K. Xi, Rational regulating pore structures of covalent organic frameworks for sulfur hexafluoride capture and separation, *Sep. Purif. Technol.*, 2023, **306**, 122595.
8. Q. Liao, C. Ke, X. Huang, D. Wang, Q. Han, Y. Zhang, Y. Zhang and K. Xi, A Versatile Method for Functionalization of Covalent Organic Frameworks via Suzuki–Miyaura Cross-Coupling, *Angew. Chem. Int. Ed.*, 2021, **60**, 1411-1416.
9. Y. Yin, Y. Zhang, X. Zhou, B. Gui, G. Cai, J. Sun and C. Wang, Single-Crystal Three-Dimensional Covalent Organic Framework Constructed from 6-Connected Triangular Prism Node, *J. Am. Chem. Soc.* , 2023, **145**, 22329-22334.
10. S. Tong, L. Yao, Q. Wang, J. Zhu, Z. Wang and J. Yan, Room-Temperature Synthesis of a Fluorine-Functionalized Nanoporous Organic Polymer for Highly Efficient SF_6 Adsorption and Separation, *ACS Macro Lett.* , 2024, **13**, 1469-1475.
11. J. Zhu, D. Luo, Q. Wang, S. Tong, Z. Wang and J. Yan, Room-temperature synthesis of a fluorine-functionalized nanoporous organic polymer for efficient SF_6 separation, *Chem. Commun.*, 2024, **60**, 12209-12212.
12. X. Yang, Q. Wang, J. Zhu, J. Yan and S. Guo, Non-fluorinated Triazine-Functionalized Pentiptycene-Based Nanoporous Organic Polymer for Highly Efficient SF_6/N_2 Separation, *ACS Materials Lett.* , 2025, **7**, 1940-1946.
13. J. Zhu, X. Chen, Q. Wang and J. Yan, Fluorine Density Gradient Engineering in Triazine-Based Nanoporous Organic Polymers for Highly Selective SF_6 Capture, *ACS Appl. Mater. Interfaces* 2025, **17**, 70029-70038.
14. Q. Wang, J. Zhu and J. Yan, Cooperative Binding in a Fluorinated Nanoporous Polyketaminal Network for Highly Selective SF_6 and CF_4 Capture, *ACS Macro Lett.* , 2025, **14**, 1535−1542.
15. W. Zhang, Y. Wu, Y. Li, S. Chen, Y. Fu, Z. Zhang, T. Yan, S. Wang and H. Ma, Fluorine-functionalized Porous Organic Polymers for Durable F-gas Capture from Semiconductor Etching Exhaust, *Macromolecules*, 2022, **55**, 1435-1444.
16. W. Zhang, Y. Li, S. Wang, Y. Wu, S. Chen, Y. Fu, W. Ma, Z. Zhang and H. Ma, Fluorine-Induced Electric Field Gradient in 3D Porous Aromatic Frameworks for Highly Efficient Capture of Xe and F-Gases, *ACS Appl. Mater. Interfaces* 2022, **14**, 35126-35137.

17. Y. Wu, X. Li, Y. Li, C. Tao, Y. Tang, S. Wang, Y. Fu, W. Ma, W. Zhang and H. Ma, Porous aromatic frameworks as HF resistant adsorbents for SF6 separation at elevated pressure, *Sep. Purif. Technol.*, 2023, **315**, 123657.
18. L. Yan, H.-T. Zheng, L. Song, Z.-W. Wei, J.-J. Jiang and C.-Y. Su, Methyl-functionalized flexible ultra-microporous MOF for efficient SF_6/N_2 mixture separation, *Chem. Eng. J.*, 2023, **472**, 145145.
19. M. Åhlén, A. Jaworski, M. Strømme and O. Cheung, Selective adsorption of CO_2 and SF_6 on mixed-linker ZIF-7–8s: The effect of linker substitution on uptake capacity and kinetics, *Chem. Eng. J.*, 2021, **422**, 130117.
20. S. M. Wang, X. T. Mu, H. R. Liu, S. T. Zheng and Q. Y. Yang, Pore-Structure Control in Metal–Organic Frameworks (MOFs) for Capture of the Greenhouse Gas SF6with Record Separation, *Angew. Chem. Int. Ed.*, 2022, **61**, e202207066.
21. Y.-P. Li, J.-J. Ni, S. Li, J. Wang, Z.-Y. Sui and X.-F. Xu, Rational pore-window size control in three Cu-MOFs with different pore environments for efficient capture of the greenhouse gas SF_6, *J. Solid State Chem.*, 2024, **329,** 124443.
22. T. Meng, E. Wang, Y. Peng, Z. Li, H. Lei, S. Chaleawlert-umpon, H. Su, Y. Wang and L. Li, Dichloromethane-knitting synthesis of fluorinated porous organic polymers for superior sulfur hexafluoride adsorption and separation, *Sep. Purif. Technol.*, 2025, **369**, 133024.
23. Y. Zhao, C. Meng, Y. Chen, W. Gong, G. Xing, D. Yuan and T. Ben, tert-Butyl Functionalized Ultra-Microporous Three-Dimensional Covalent Organic Framework for Efficient SF_6/N_2 Separation, *Angew. Chem. Int. Ed.*, 2025, **64**, e202508493.